

Supporting Information

Enhanced Oxygen Evolution Catalyzed by In-Situ Formed Fe-Doped Ni Oxyhydroxides in Carbon Nanotubes

Dandan Chen^[a], QiuHong Sun^[a], Cheng Han^[a], Yuanyuan Guo^[a], Qi Huang^[a], William
A. Goddard, III^{*[b]} and Jinjie Qian^{*[a,b]}

^aKey Laboratory of Carbon Materials of Zhejiang Province, College of Chemistry and
Materials Engineering, Wenzhou University, Wenzhou, Zhejiang, 325035, P. R. China

^bMaterials and Process Simulation Center (MSC), MC 139-74, California Institute of
Technology, Pasadena, California 91125, United States

*Corresponding author

E-mail: jinjieqian@wzu.edu.cn; wag@caltech.edu

Experimental Section

Chemicals and Reagents

All chemicals are purchased and used without further purification. Nickel(II) acetate tetrahydrate ($\text{Ni}(\text{CH}_3\text{COO})_2 \cdot 4\text{H}_2\text{O}$, 99.9%), Ferric (III) sulfate ($\text{Fe}_2(\text{SO}_4)_3 \cdot x\text{H}_2\text{O}$, 99.95%), Potassium thiocyanate (KSCN, 98.5%), biphenyl-3,3',5,5'-tetracarboxylic acid (H_4BPTC , 98.0%, Jinan Henghua Technology Company), urea ($\text{CH}_4\text{N}_2\text{O}$, 99%), N-Methylformamide (NMF, 99%), triethylamine (TEA, 99%), Nitric acid concentrated solution (HNO_3 , 70%) and ethanol (EtOH, 95%), are purchased from Aladdin. 5 wt% Nafion ionomer are purchased from Aldrich. All the salts, solvents and other reagents are of analytical grade. High-purity N_2 , Ar gases, and de-ionized water (18 M Ω) are used in all experiments.

Experimental

Synthesis of NiOF-1

Add $\text{Ni}(\text{CH}_3\text{COO})_2 \cdot 4\text{H}_2\text{O}$ (60 mg), H_4BPTC (15 mg), NMF (3 mL), H_2O (1 ml), TEA (0.1 ml) and HNO_3 (0.1 ml) to a 35 mL stress-tolerant glass tube. Then the pressure tube is placed into an aluminum model holding at 140 °C for 2 hours. The crystals of **NiOF-1** are obtained by further washing with ethanol for 3 times. Based on the used organic ligand, the yield of **NiOF-1** is calculated to be about 60.1%, and the repeatability is excellent.

Synthesis of NiOF-1-Fe

Add **NiOF-1** (30 mg), $\text{Fe}_2(\text{SO}_4)_3 \cdot x\text{H}_2\text{O}$ (15 mg) and ethanol (10 mL) to a 25 mL reaction kettle. Then the kettle is placed into an oven holding at 120 °C for 6 hours. The

Ni-Fe-hollow nanoparticles (denoted as **NiOF-1-Fe**) are obtained by further washing with ethanol for 3 times.

Synthesis of Ni@C and FeNi₃@C

The nanorod structures of **NiOF-1** and hollow **NiOF-1-Fe** are weighed and placed on drivepipes, and further placed in a CVD tube furnace for the following thermal treatment. The temperature is set to 800 °C at a heating rate of 10 °C min⁻¹ under an Ar (50 sccm) atmosphere, and it is maintained at a constant temperature for another 2 hours. The black powders are obtained after falling to room temperature, denoted as Ni@C and FeNi₃@C, respectively.

Synthesis of Ni@NCNT and FeNi₃@NCNT

The nanorod structures of **NiOF-1** and hollow **NiOF-1-Fe** are weighed and placed them together with tenfold CH₄N₂O on the drivepipes, then further placed in a CVD tube furnace for the following thermal treatment. The temperature is set to 800 °C at a heating rate of 10 °C min⁻¹ under an Ar (50 sccm) atmosphere, and it is maintained at a constant temperature for another 2 hours. The black powders are obtained after falling to room temperature, denoted as Ni@NCNT and FeNi₃@NCNT, respectively. After carbonization at 800 °C, FeNi₃@NCNT can maintain about 25.1% of precursor mass.

Material Characterization

The products are characterized by using scanning electron microscopy (SEM) on a JEOL JSM 6700F microscope, transmission electron microscopy (TEM) on an FEI Tecnai F20 electron microscope, high-resolution transmission electron microscope and energy dispersive X-ray spectroscopy (EDS) analyses are carried out under JEOL JEM-

2100F microscope operating at an accelerating voltage of 200 kV. And powder X-ray diffraction (PXRD) (D/Max2000, Rigaku) using a Bruker D8-Advance powder diffractometer operates at 40 kV, 40 mA for Cu K α radiation ($\lambda = 1.5406 \text{ \AA}$). Raman spectrometer (LabRAM HR Evolution) is used to investigate the phase composition of samples at GS1000. Raman spectrometer (LabRAM HR Evolution) is used to investigate the phase composition of samples at GS1000. Fourier transform infrared spectroscopy (FT-IR) spectra are carried on in the model of PerkinElmer Frontier MIR. Thermal gravimetric analysis (TGA) is performed on a NETZSCH STA 449C instrument where pure nitrogen as a carrier gas with a heating rate of $10 \text{ }^\circ\text{C min}^{-1}$. X-ray photoelectron spectroscopy (XPS) is conducted on a Thermo Scientific ESCALAB 250. Nitrogen sorption analysis is performed at 77 K using a Micromeritics ASAP 2020 surface-area and pore-size analyzer. The specific surface areas are calculated by using the Brunauer-Emmett-Teller (BET) equation from the nitrogen adsorption data in the relative range (P/P_0) of 0.04-0.2. The pore size distribution (PSD) plots are obtained from the adsorption and desorption branch of the isotherm based on the Barrett-Joyner-Halenda (BJH) model and/or Horvath-Kawazoe (H-K) models.

Electrochemical measurements

The electrochemical experiments are carried out at room temperature using a CHI 760E electrochemical station for OER. The experiment used the electrodes of Hg/Hg₂Cl₂ and platinum net are sequentially behaved as the reference (RE) and counter electrodes (CE), which are used in 1.0 M KOH electrolyte solution. According to a formula $E_{\text{RHE}} = E_{\text{SCE}} + 0.242 \text{ V} + 0.059 \text{ V} \times \text{pH} = E_{\text{SCE}} + 1.05$, all of its potentials can be corrected to

reversible hydrogen electrode (RHE) potentials. In a mixture solution of 500 μL of 3:2 v/v distilled water/ethanol, and 5 wt % Nafion solution (30 μL), the catalyst powder (5 mg) is dispersed to form a homogeneous catalyst ink after 2 h' sonication. Thereafter, the surface of glassy carbon (diameter: 3 mm) is loaded with 10 μL of a catalyst ink, wherein 1.3 mg cm^{-2} is calculated the loading amount. Linear sweep voltammetry (LSV) is conducted in electrolyte solution without correction (a scan rate: 5 mV s^{-1}). The Tafel slope is transferred according to Tafel equation as follows: $\eta = b \cdot \log(j / j_0)$. Regarding the evaluation of the electrochemical active surface areas (ECSA) of the samples, CV has also been performed by measuring the double-layer capacitances (C_{dl}) with various scan rate (20, 40, 60, 80, 100 and 120 mV s^{-1}) under the potential window of 1.15-1.25 V vs. RHE. Under the constant voltage, the EIS is performed to test the range of from 100 kHz to 0.01 Hz. For evaluating the long-term performance, the electrochemical stability of the catalyst is conducted at a constant overpotential for achieving a high initial current density. In order to calculate the electron transfer number, RRDE voltammogram of **FeNi₃@NCNT** is conducted to collect disk current and ring current at the same time. Faradaic efficiency, the ring potential is held constantly at 0.40 V vs. RHE to reduce the emerged O_2 on the disk electrode at a rotation rate of 1600 rpm in N_2 -saturated 1.0 M KOH. Oxygen is generated by OER with a constant current on the disk electrode. Faradaic efficiency can be calculated by the collection efficiency of disk current, ring current and disc-ring electrode. The produced O_2 gas is also collected to evaluate the real-time rate of O_2 generation and Faraday efficiency of as-prepared catalysts at 1.50 V, O_2 gases are quantitatively analyzed every

5 minutes by Ocean Optics' standard oxygen sensors, which is designed for monitoring oxygen partial pressure in gas and aqueous solutions. In this system, all electrochemical tests are performed without iR-corrected.

Simulation Details

In this work, the projector augmented wave (PAW) method to model the valence electron-ion interactions is employed for all calculations. We use periodic (100) slab models consisting of four metal-oxygen layers with three metal sites per layer, which has been considered as the OER active surface in similar oxide models. The slabs are separated by a 15 Å vacuum region and the atomic positions of top two layers are optimized while other two layers are fixed at the optimized bulk position. The Γ -centered ($3\times 3\times 1$) Monkhorst-Pack K-point grids and a plane-wave energy cutoff of 400 eV are used for the slab calculations. In addition, the vibrational frequencies are computed to include the zero-point energies, enthalpy, and entropy to ultimately calculate the free energies at room temperature (298.15 K). After the geometry optimization of the slab for NiOOH, we found that 1/3 of the Ni atoms (the ones close to K^+ ions) have oxidation state of +3, probably due to the K^+ ions donating to the nearest Ni. Thus 2/3 of the Ni atoms have 4^+ oxidation states, leading to an average oxidation state of +3.67 for Ni, in agreement with previous reports.

Crystal Data and Refinement Results

Table S1. Single Crystal X-Ray Data for Rod-Like NiOF-1.

Compound	NiOF-1^{Ref.1-2}
Chemical formula	NiC ₈ H ₃ O ₆
Formula mass	253.81
Crystal system	Tetragonal
Space group	I4 ₁ 22
a (Å)	15.1780(5)
b (Å)	15.1780(5)
c (Å)	12.0813(5)
α (°)	90
β (°)	90
γ (°)	90
Unit cell volume (Å³)	2783.19(18)
Temperature (K)	293(2)
Z	8
F(000)	1016
No. of reflections measured	2606
R_{int}	0.0732
Final R₁ values (I>2σ(I))	0.0691
Final wR (F₂) values (I>2σ(I))	0.1735

Ref. 1-2: For more details on the crystal structure data, please see the previously published works, e.g. *J. Mater. Chem. A*, 2016,4, 16198-16204; *Chem. Commun.*, 2012,48, 9696-9698.

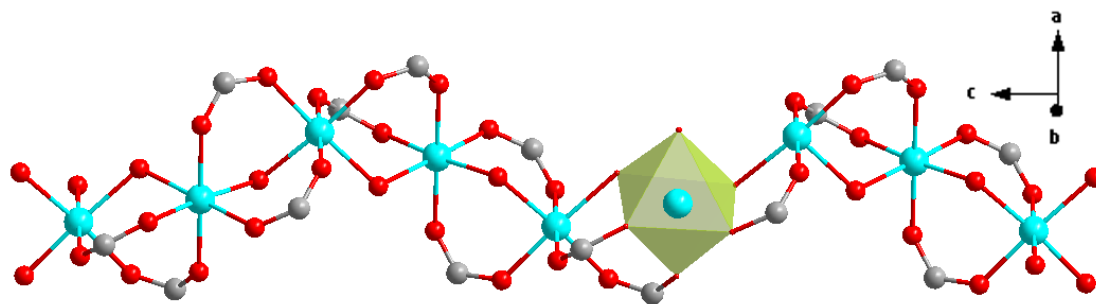


Figure S1. 1-dimensional Ni-O chain and 6-coordinated octahedron geometry of Ni(II) centers in NiOF-1.

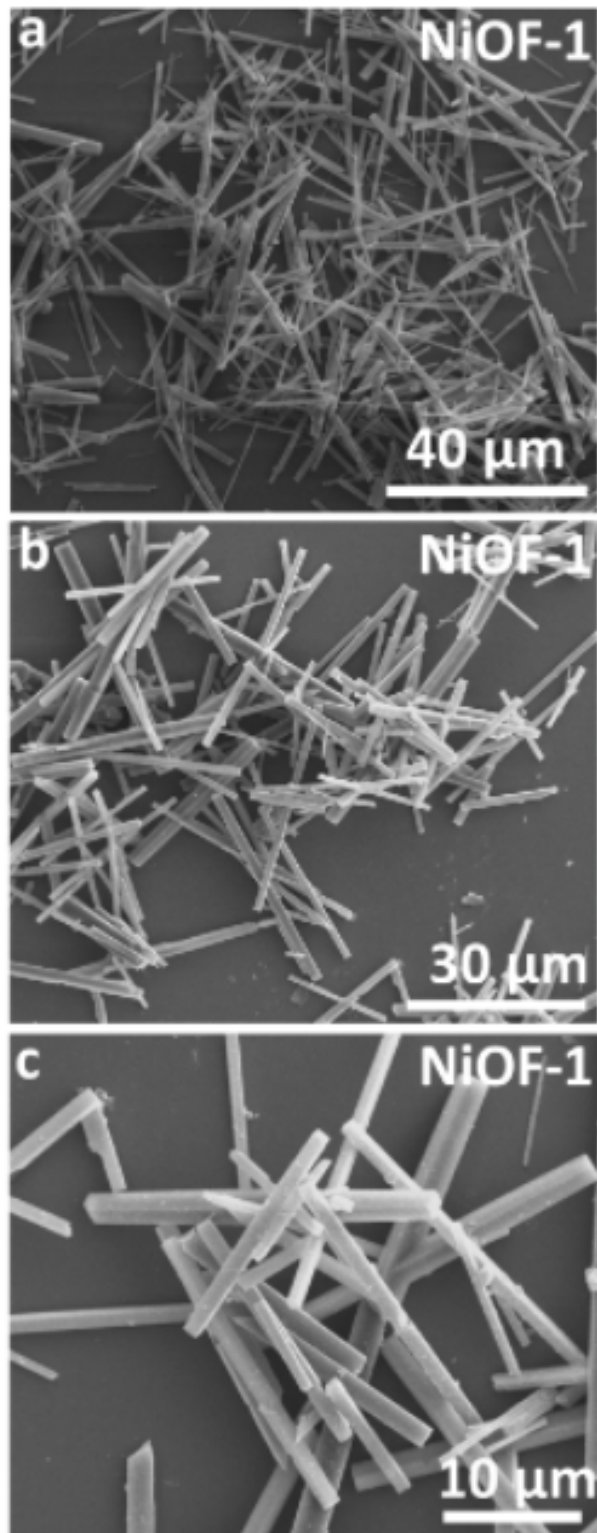


Figure S2. SEM images of (a-c) NiOF-1.

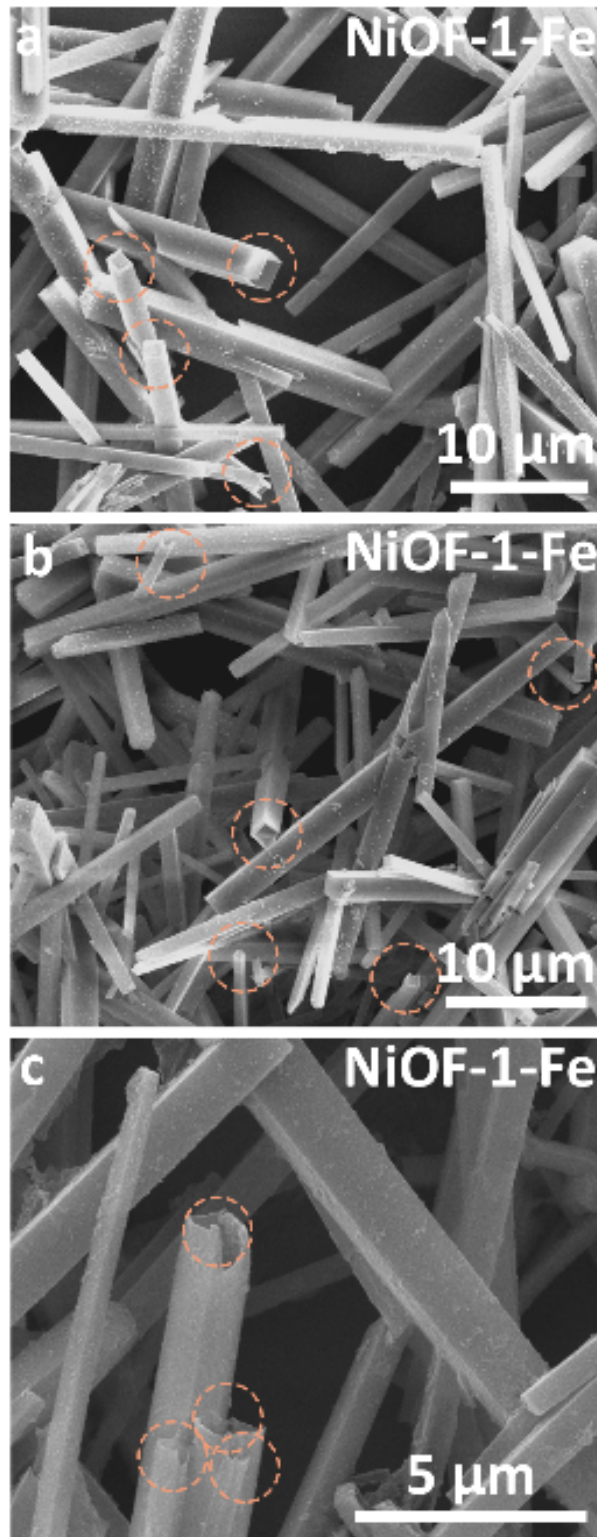


Figure S3. SEM images of (a-c) hollow NiOF-1-Fe.

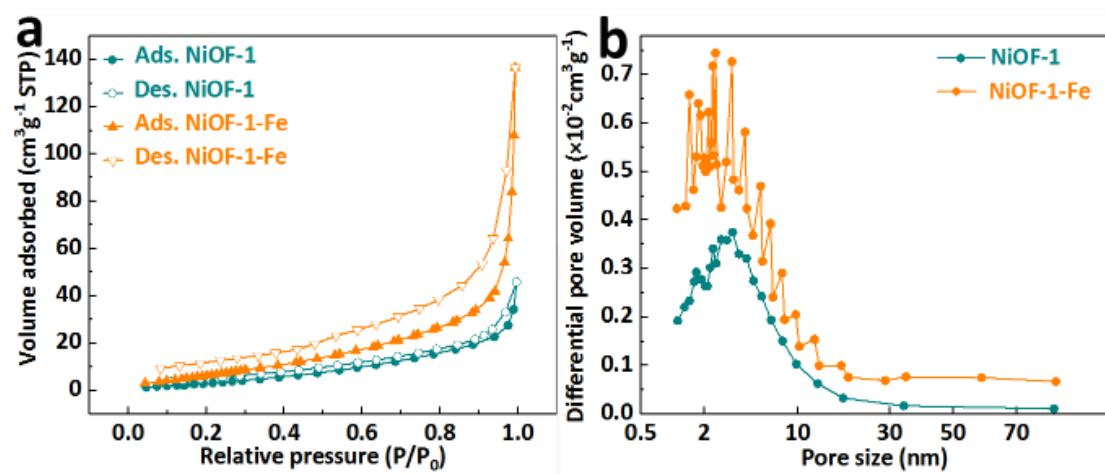


Figure S4 (a) Nitrogen isotherms at 77 K and (b) the corresponding PSD curves of NiOF-1 and NiOF-1-Fe.

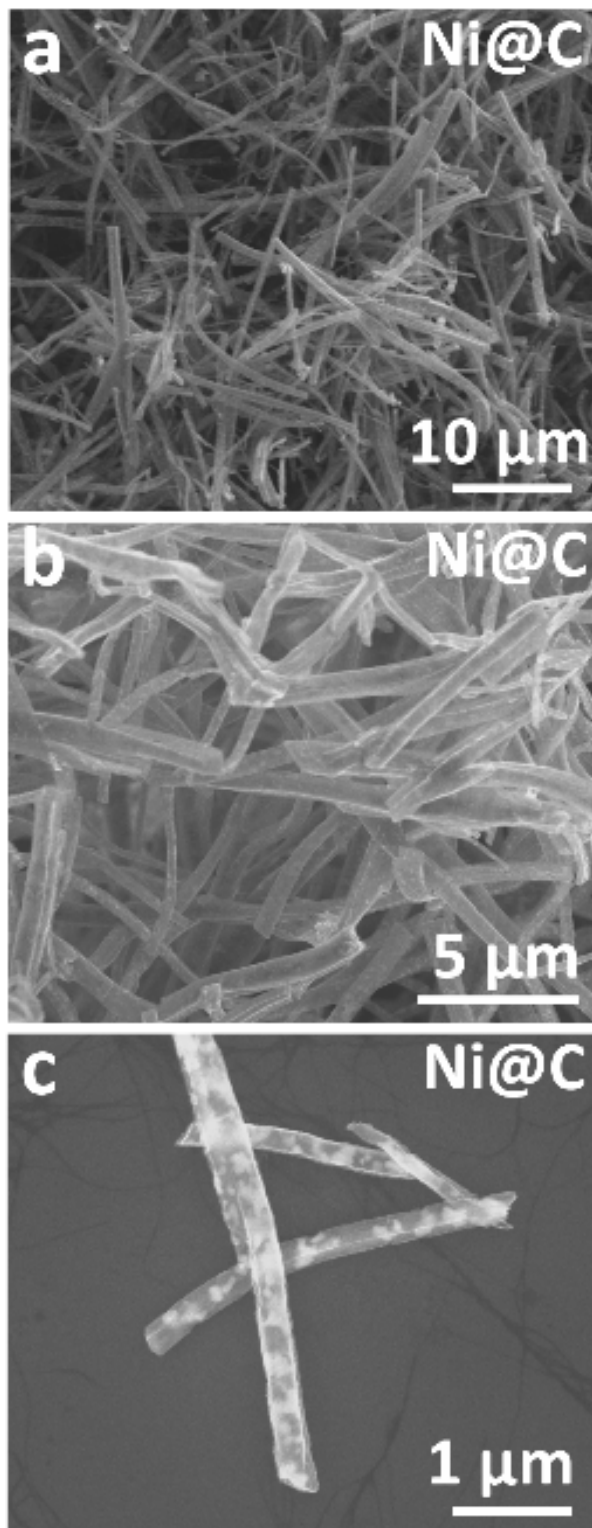


Figure S5. SEM images of (a-c) Ni@C.

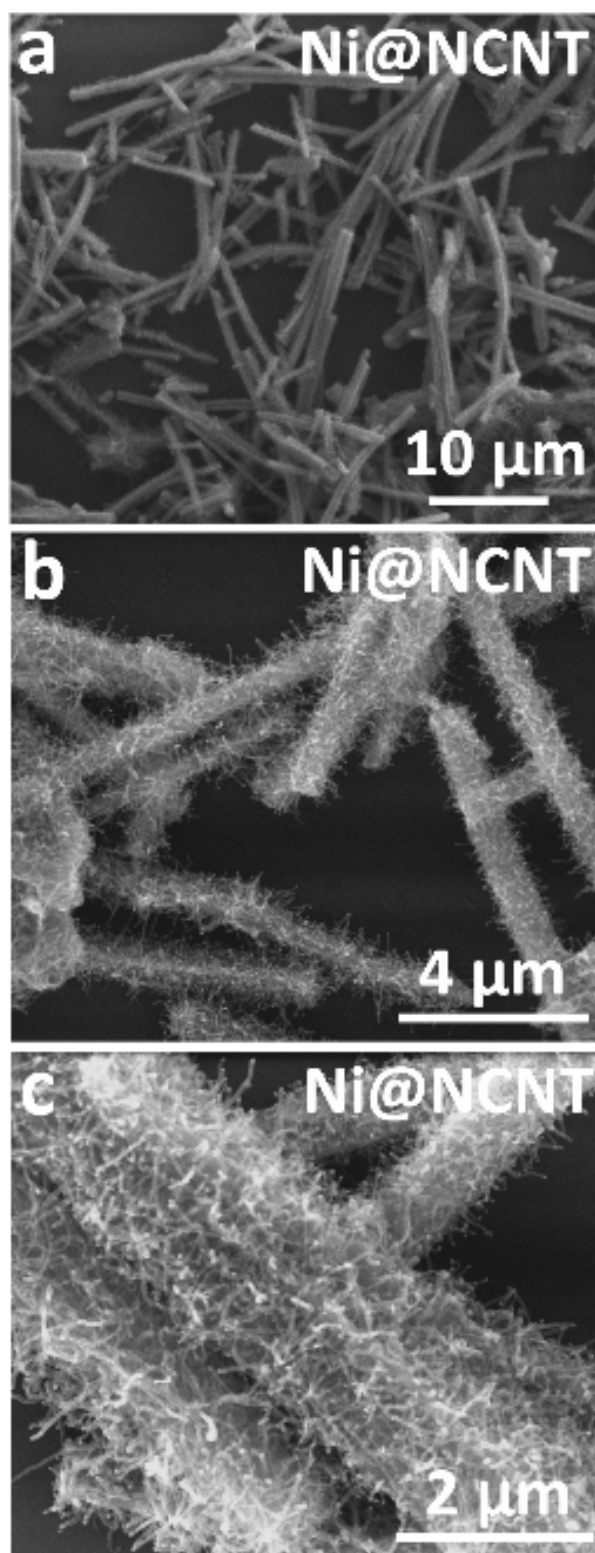


Figure S6. SEM images of (a-c) Ni@NCNT.

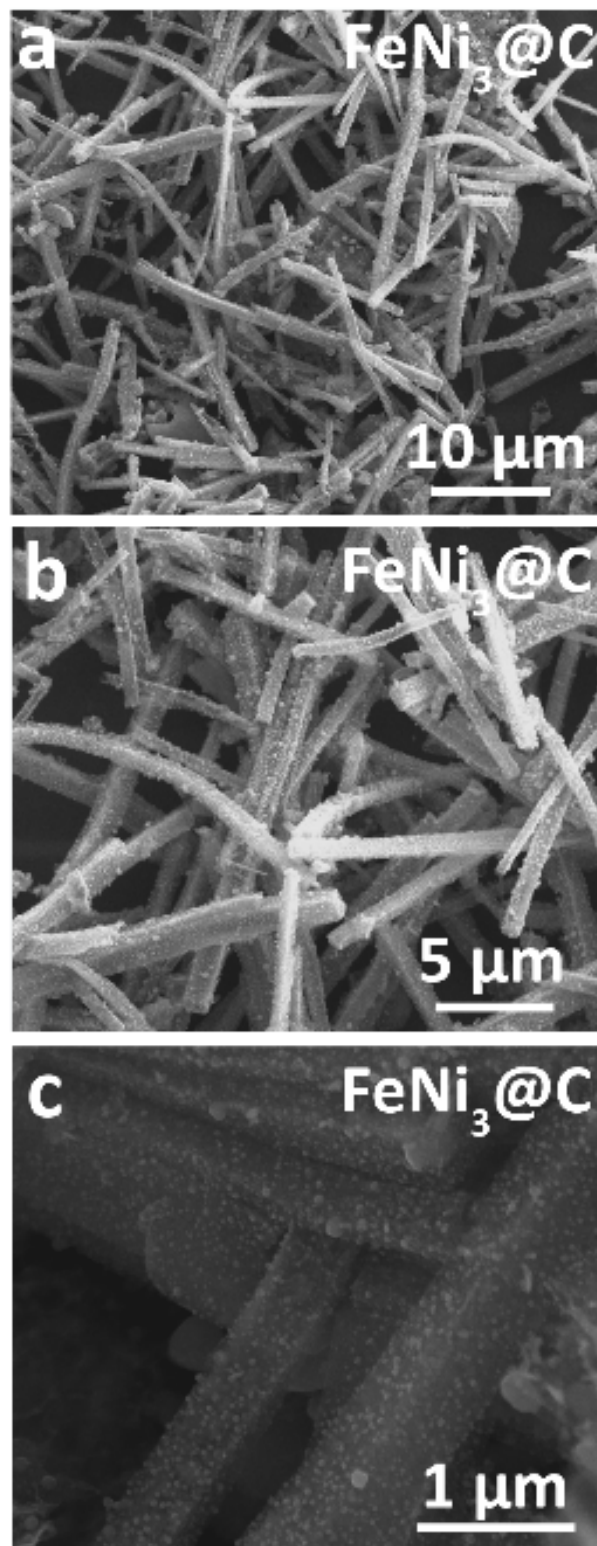


Figure S7. SEM images of (a-c) FeNi₃@C.

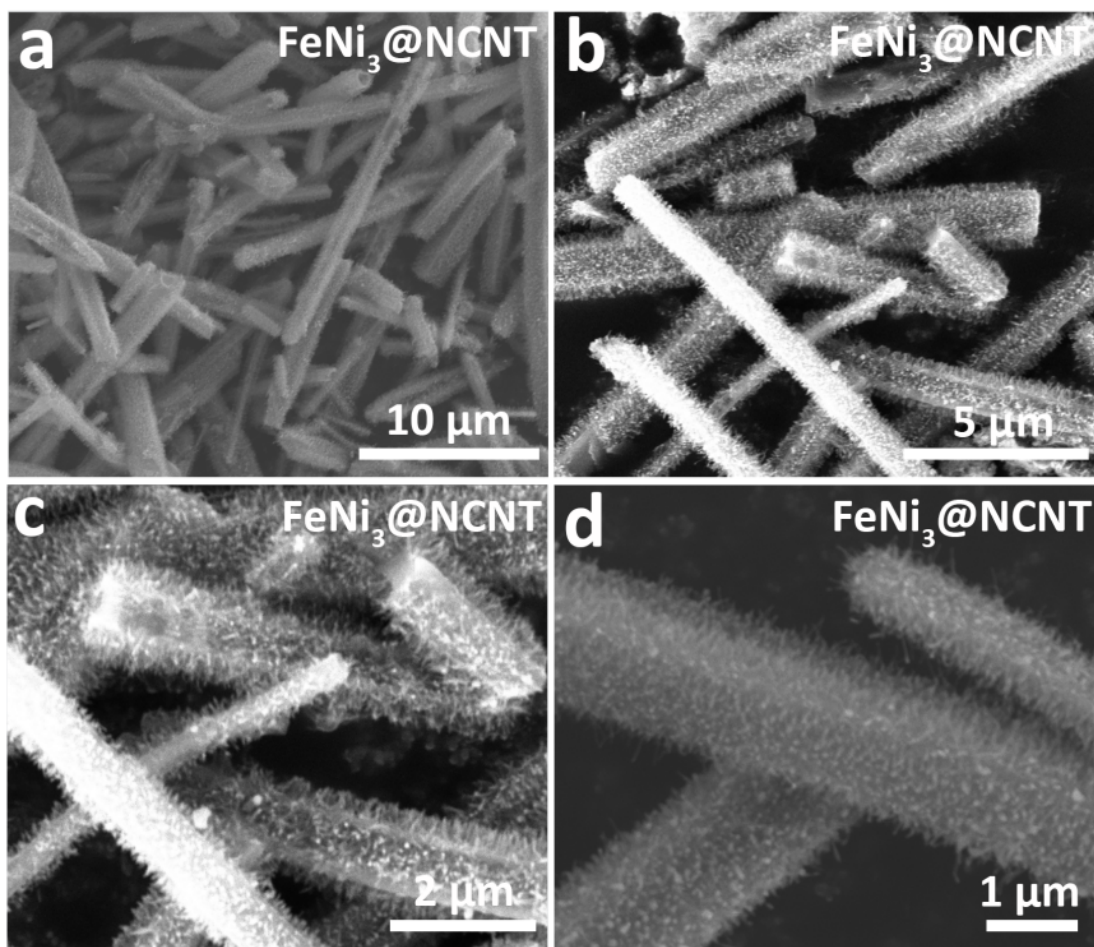


Figure S8. SEM images of (a-d) FeNi₃@NCNT.

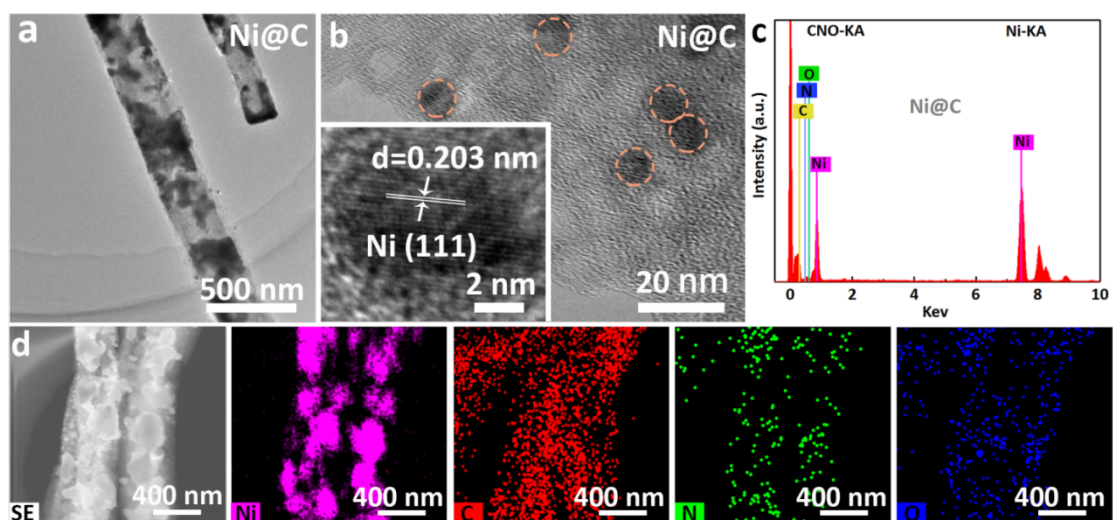


Figure S9. (a) TEM image, (b) HR-TEM image, (c) EDX spectrum, (d) HAADF-STEM image and corresponding element mappings showing the distribution of Ni, C, N, and O of Ni@C.

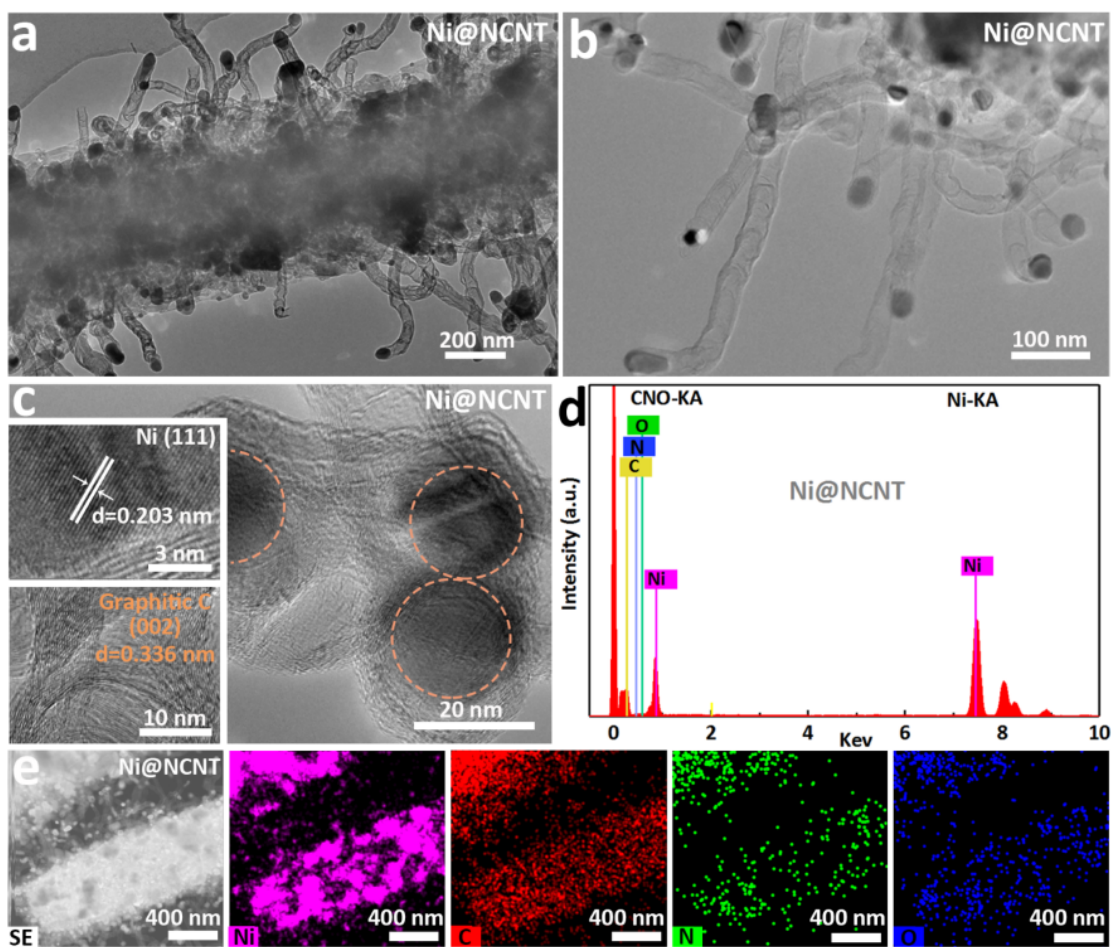


Figure S10. (a-b) TEM image, (c) HR-TEM image, (d) EDX spectrum, and (e) HAADF-STEM image and corresponding element mappings showing the distribution of Ni, C, N, and O of Ni@NCNT.

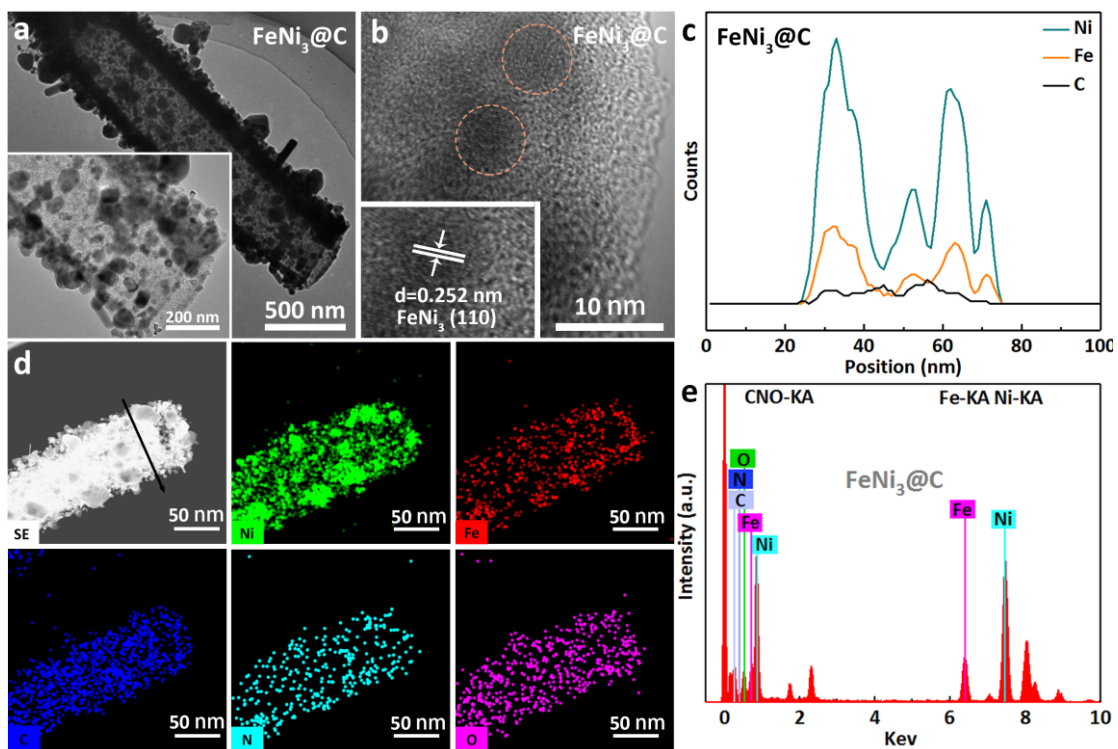


Figure S11. (a) TEM image, (b) HR-TEM image, (c) Height profiles of a single $\text{FeNi}_3@C$, (d) HAADF-STEM image and corresponding element mappings showing the distribution of Ni, C, N, and O, (e) EDX spectrum of $\text{FeNi}_3@C$.

Table S2. Summary of Pore Characteristics of NiOF-1, NiOF-1-Fe, Ni@C, Ni@NCNT, FeNi₃@C, and FeNi₃@NCNT.

Samples	Surface area/m ² g ⁻¹		Total pore volume ^a /cm ³ g ⁻¹	Micropore volume ^b /cm ³ g ⁻¹
	BET	Langmuir		
NiOF-1	15.41	31.27	0.0558	0.0034
NiOF-1-Fe	31.53	64.22	0.1696	0.0071
Ni@C	47.61	104.38	0.2267	0.0102
Ni@NCNT	67.76	123.57	0.2398	0.0186
FeNi ₃ @C	85.28	187.48	0.2109	0.0340
FeNi ₃ @NCNT	101.37	397.75	0.3775	0.0108

a At P/P₀=0.99.

b Determined by H-K (Original) method.

Table S3. Elemental Analyses Based on EDX and XPS Results.

Samples	Ni (%)		Fe (%)		C (%)		N (%)		O (%)	
	Wt.	At.	Wt.	At.	Wt.	At.	Wt.	At.	Wt.	At.
Ni@C	3.32	1.05	/	/	86.02	92.42	4.10	1.79	6.56	4.74
Ni@NCNT	3.03	1.01	/	/	82.60	92.00	7.86	2.61	6.51	4.38
FeNi₃@C	3.48	1.55	1.20	1.12	67.15	85.95	3.51	1.41	24.66	9.97
FeNi₃@NCNT	3.08	1.02	0.60	0.71	71.76	86.15	14.92	6.22	9.64	5.90

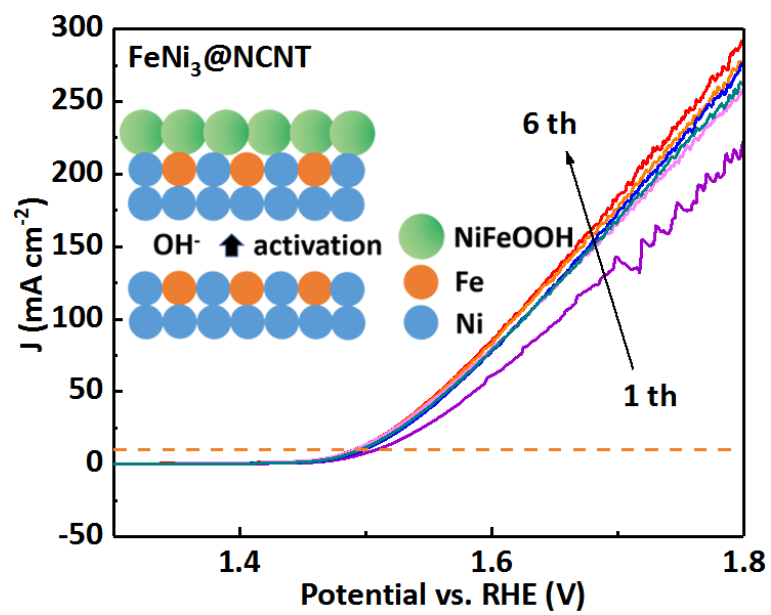


Figure S12. LSV trends of FeNi₃@NCNT in the first 6 cycles.

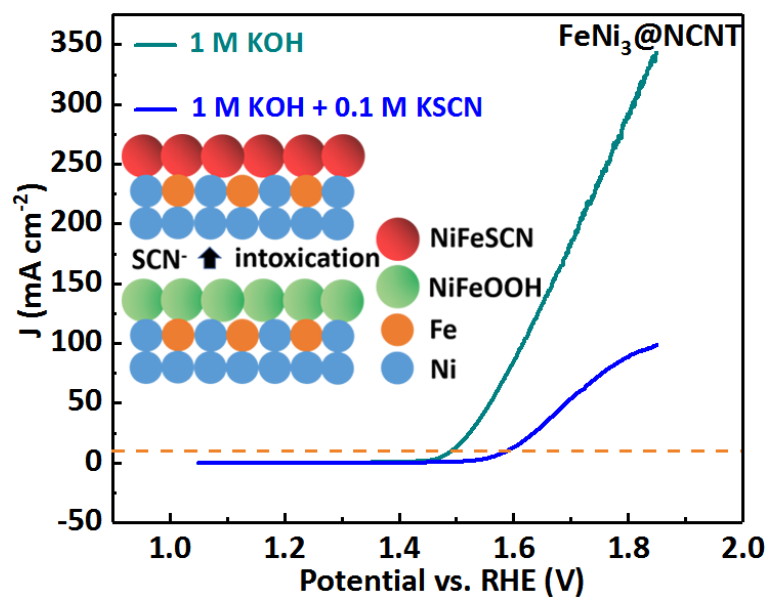


Figure S13. Polarization curves of FeNi₃@NCNT tested in 1.0 M KOH electrolyte containing 0.1 M KSCN.

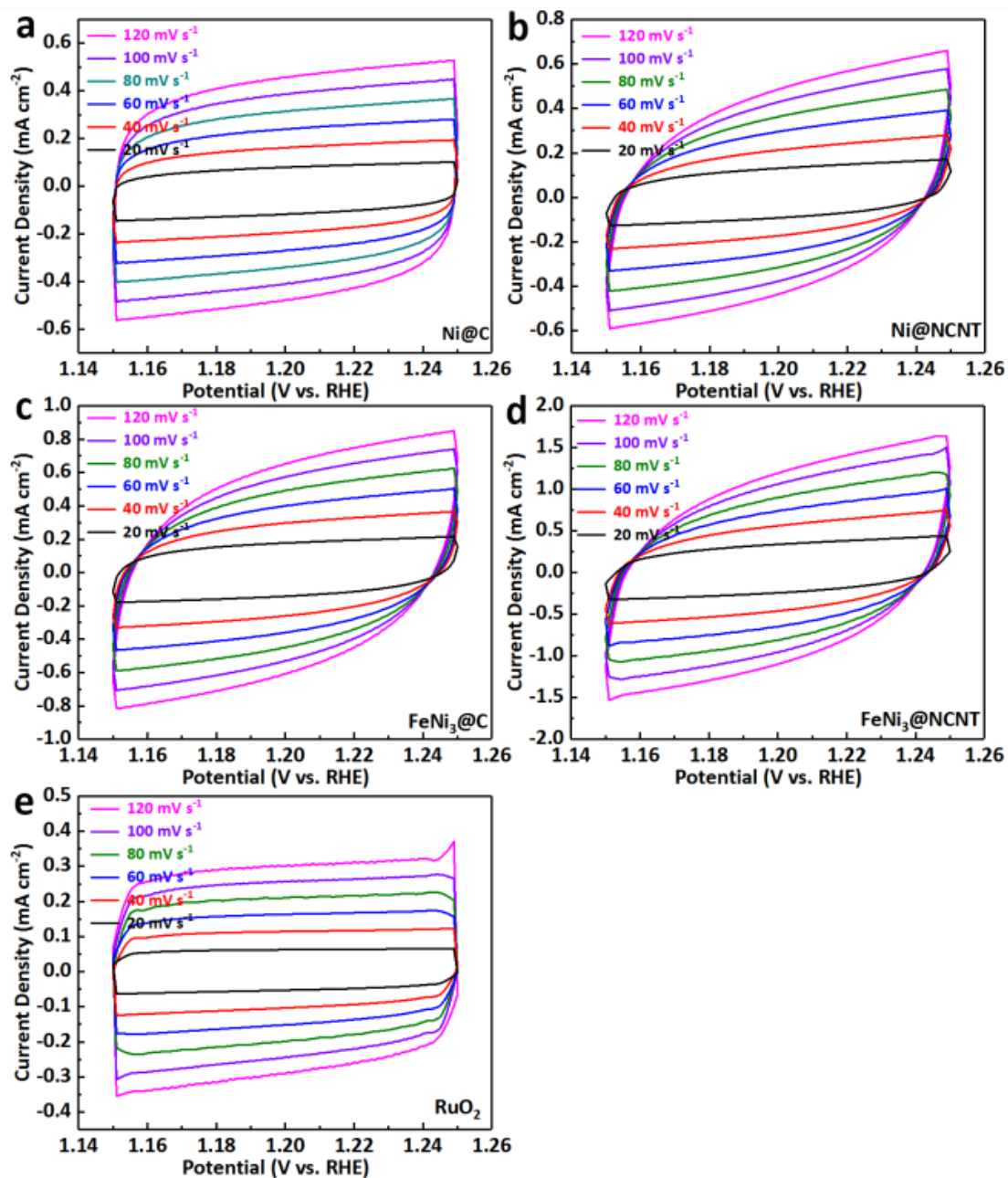


Figure S14. CV curves from 20 to 120 mV s⁻¹ of (a) Ni@C, (b) Ni@NCNT, (c) FeNi₃@C, (d) FeNi₃@NCNT and (e) RuO₂ in 1.0 M KOH.

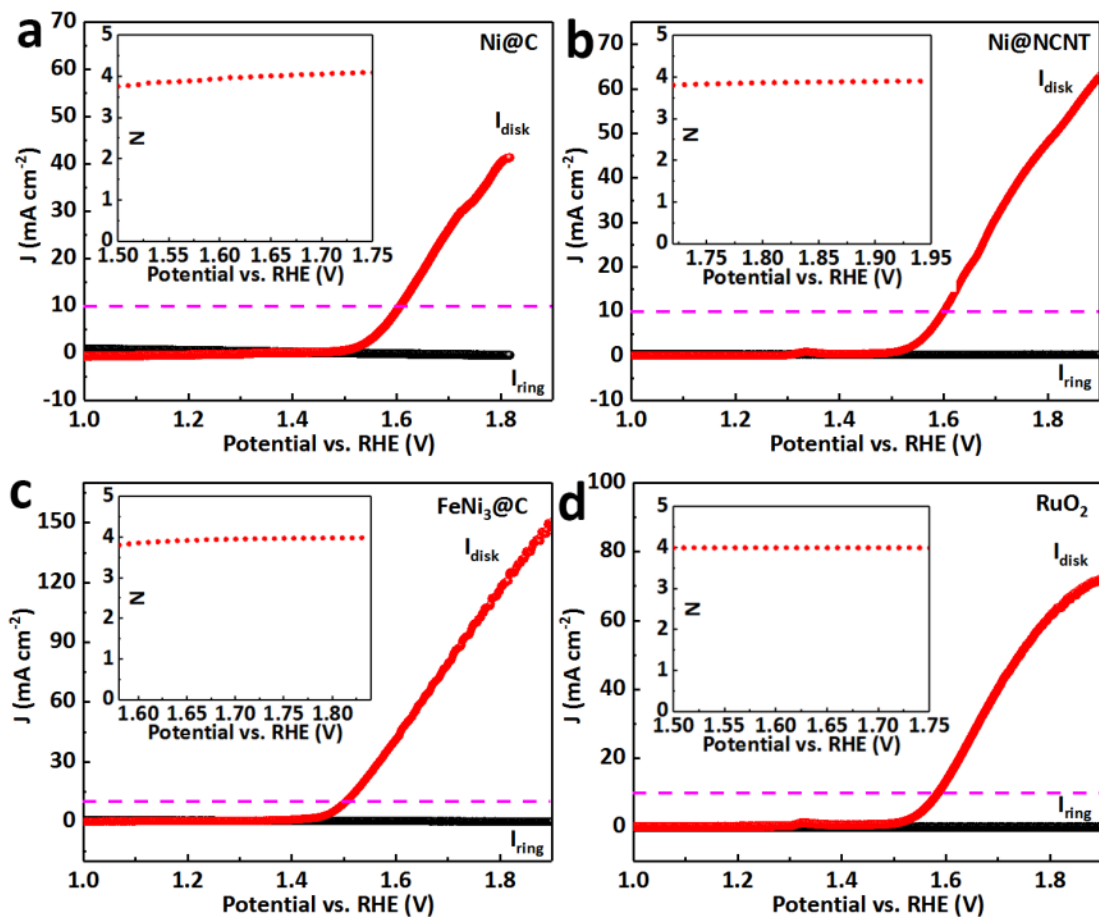


Figure S15. RRDE voltammogram of (a) Ni@C, (b) Ni@NCNT, (c) FeNi₃@C and (d) RuO₂ in 1.0 M O₂-saturated KOH electrolyte and inset shows the corresponding electron transfer number.

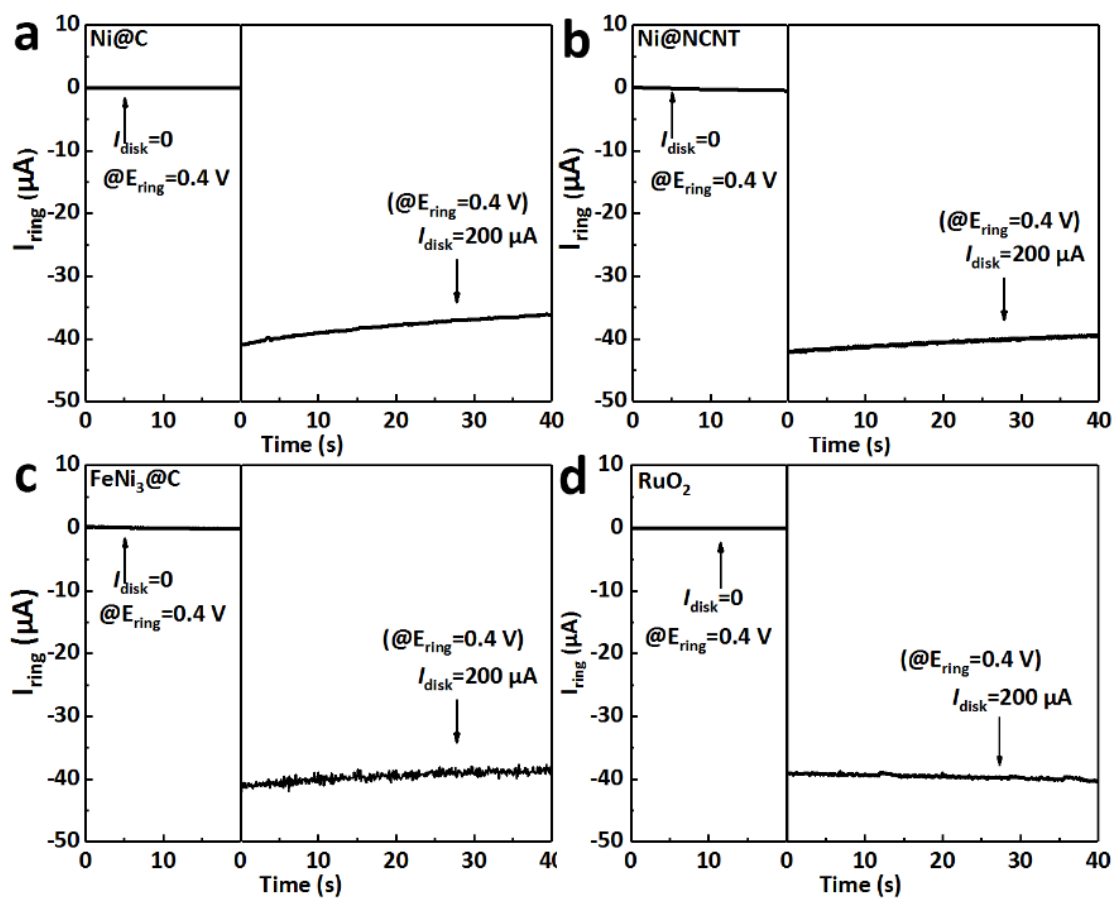


Figure S16. Ring current of Ni@C, Ni@NCNT, FeNi₃@C and RuO₂ on an RRDE in 1.0 M N_2 -saturated KOH electrolyte.

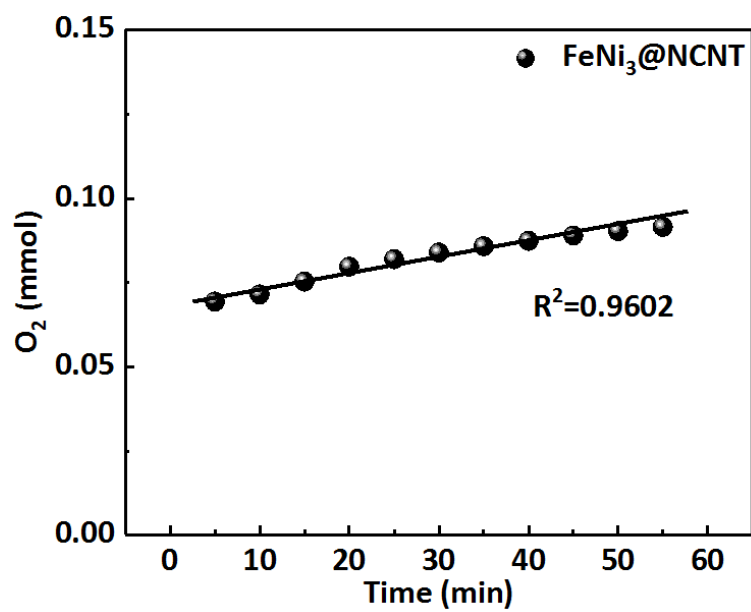


Figure S17. Experimental amounts of O₂ gas by NeoFox.

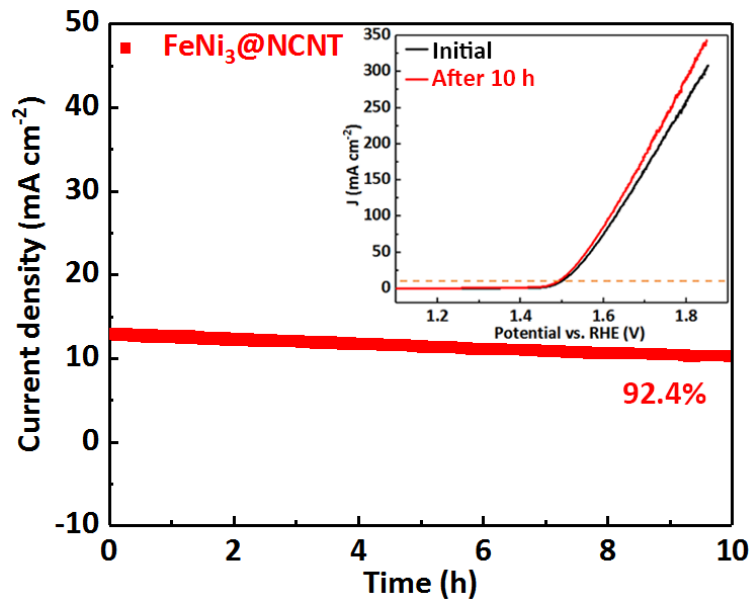


Figure S18. OER stability test of FeNi₃@NCNT for 10 h (inset LSV curves of the FeNi₃@NCNT before and after stability test).

Table S4. Electrochemical Parameters of Ni@C, Ni@NCNT, FeNi₃@C, FeNi₃@NCNT and RuO₂.

Samples	η_{10} (mV)	Tafel slope (mV dec⁻¹)	C_{dl} (mF cm⁻²)	R_{ct} (Ω)
Ni@C	360	94.6	10.11	1790.1
Ni@NCNT	351	87.1	3.68	700.8
FeNi₃@C	272	83.6	3.81	59.2
FeNi₃@NCNT	264	58.5	5.19	34.4
RuO₂	301	76.2	2.45	63.3

Table S5. OER Performance Comparison between FeNi₃@NCNT and Other Electrode Materials.

Samples	Electrolyte	η_{10} (mV)	Tafel slope (mV dec ⁻¹)	Ref.
FeNi₃@NCNT	1.0 M KOH	264	58.5	This work
FeNi ₃ @NC	1.0 M KOH	277	77	Ref. ³
NiFeC-800-5	1.0 M KOH	269	72	Ref. ⁴
Fe _{0.2} Ni _{0.8} /NC-600-a	1.0 M KOH	$\eta_{20}=290$	76	Ref. ⁵
Fe-Ni@NC-CNTs	1.0 M KOH	274	45.47	Ref. ⁶
CoNi1@C	1.0 M KOH	335	55.6	Ref. ⁷
CoP-NC@NFP	1.0 M KOH	270	84	Ref. ⁸
Co-CNT/PC	1.0 M KOH	315	73.8	Ref. ⁹
FeCoSe@NCNSs	1.0 M KOH	320	95.1	Ref. ¹⁰
NiFeP/NF	1.0 M KOH	255	41	Ref. ¹¹
Fe-Ni ₃ S ₂ /FeNi	1.0 M KOH	282	54	Ref. ¹²
Fe1Co1-P/C	1.0 M KOH	360	58.4	Ref. ¹³
CdP2-CDs-CoP	1.0 M KOH	285	81.77	Ref. ¹⁴
FeNiF/NCF	1.0 M KOH	260	67	Ref. ¹⁵
FeNi ₃ /M-C-800	1.0 M KOH	246	40	Ref. ¹⁶
FeCo/FeCoNi@NCNTs-HF	0.1 M KOH	378	57	Ref. ¹⁷
Fe-FeNi ₃ /NC	0.1 M KOH	360	82	Ref. ¹⁸

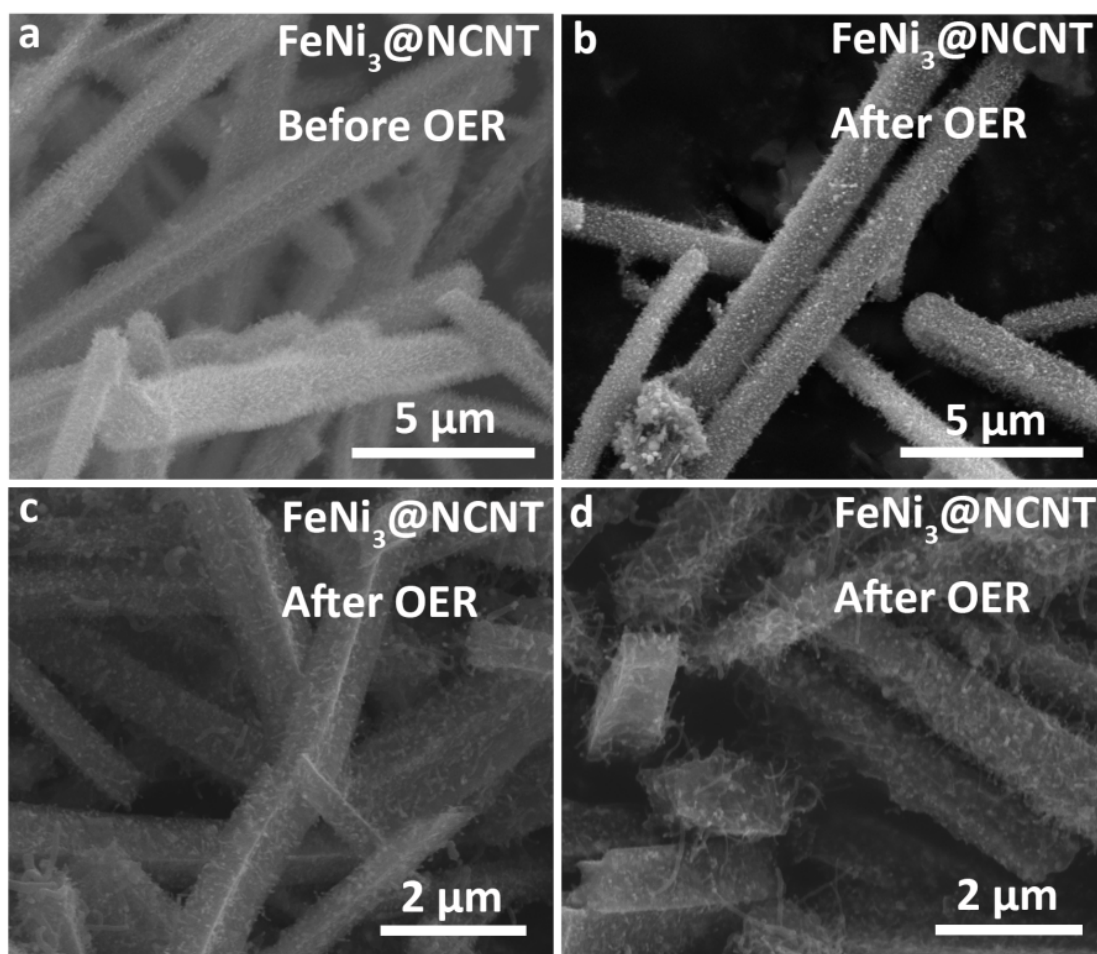


Figure S19. SEM images of FeNi₃@NCNT (a) before and (b-d) after OER.

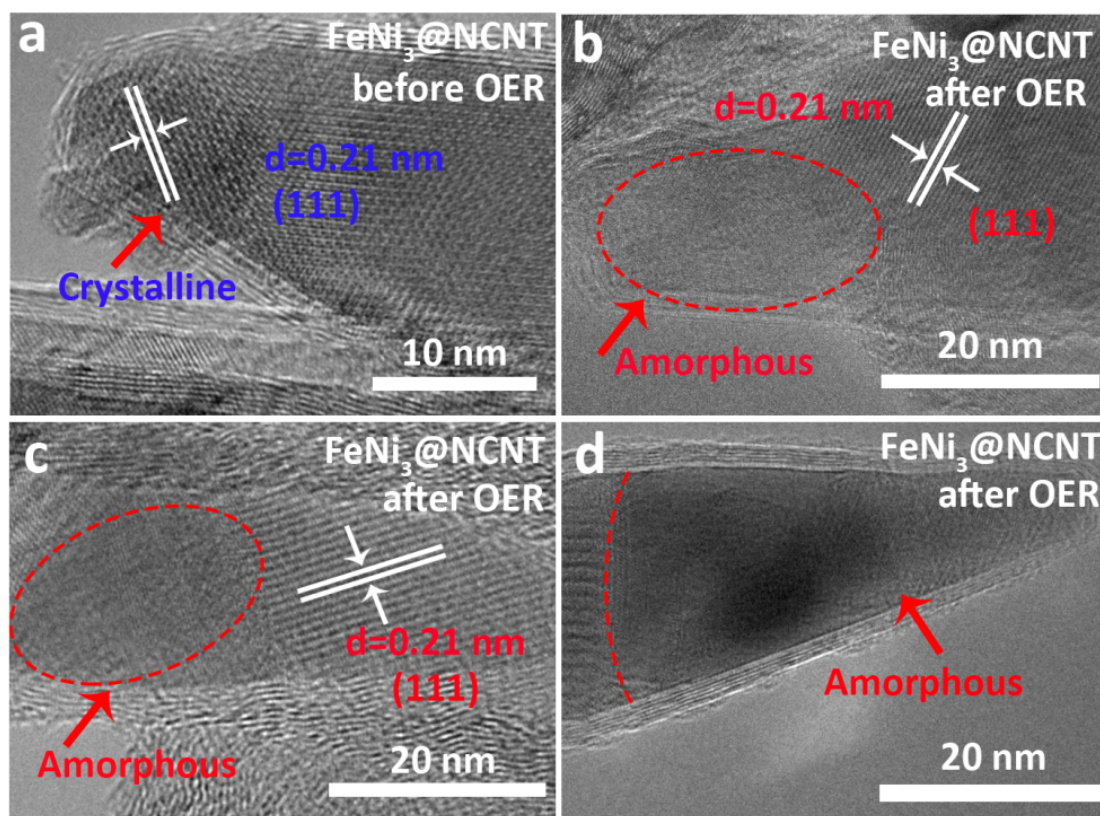


Figure S20. HR-TEM images of FeNi₃@NCNT (a) before and (b-d) after OER.

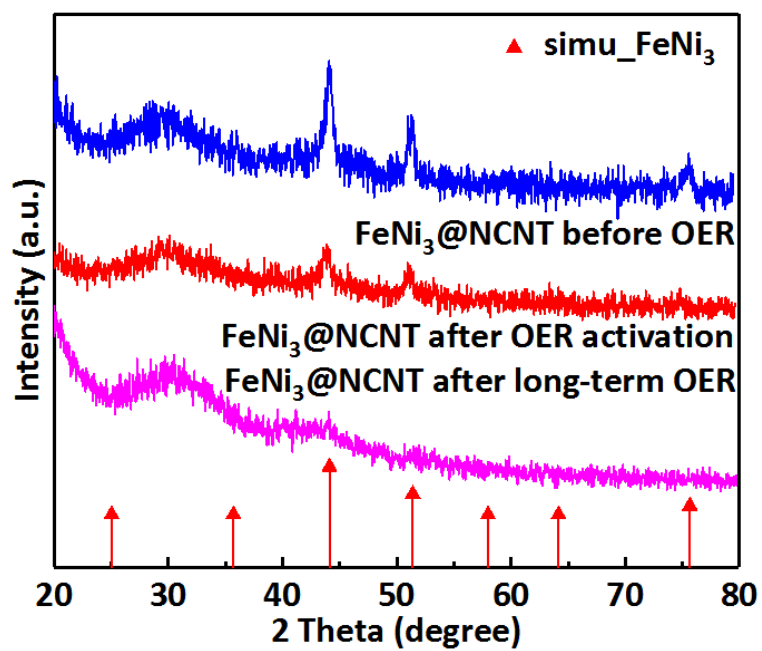


Figure S21. PXRD pattern of FeNi₃@NCNT before and after OER.

References:

1. Zhang, X.; Chen, W.; Shi, W.; Cheng, P., Highly selective sorption of CO₂ and N₂O and strong gas-framework interactions in a nickel(II) organic material. *J. Mater. Chem. A*, **2016**, *4*, 16198.
2. Qian, J.; Jiang, F.; Yuan, D.; Wu, M.; Zhang, S.; Zhang, L.; Hong, M., Highly selective carbon dioxide adsorption in a water-stable indium-organic framework material. *Chem Commun (Camb)* **2012**, *48* (78), 9696-8.
3. Chen, D.; Zhu, J.; Mu, X.; Cheng, R.; Li, W.; Liu, S.; Pu, Z.; Lin, C.; Mu, S., Nitrogen-Doped carbon coupled FeNi₃ intermetallic compound as advanced bifunctional electrocatalyst for OER, ORR and zn-air batteries. *Applied Catalysis B: Environmental* **2020**, *268*.
4. Ding, J.; Sun, Q.; Zhong, L.; Wang, X.; Chai, L.; Li, Q.; Li, T.-T.; Hu, Y.; Qian, J.; Huang, S., Thermal conversion of hollow nickel-organic framework into bimetallic FeNi₃ alloy embedded in carbon materials as efficient oer electrocatalyst. *Electrochimica Acta* **2020**, *354*.
5. Zhou, Y.; Li, Y.; Zhang, L.; Zhang, L.; Li, L.; Tian, J.; Wang, M.; Xu, J.; Dai, B.; Li, Y., Fe-leaching induced surface reconstruction of Ni-Fe alloy on N-doped carbon to boost oxygen evolution reaction. *Chemical Engineering Journal* **2020**, *394*.
6. Zhao, X.; Pachfule, P.; Li, S.; Simke, J. R. J.; Schmidt, J.; Thomas, A., Bifunctional Electrocatalysts for Overall Water Splitting from an Iron/Nickel-Based Bimetallic Metal-Organic Framework/Dicyandiamide Composite. *Angew Chem Int Ed Engl* **2018**, *57* (29), 8921-8926.
7. Zhang, X.; Luo, J.; Wan, K.; Plessers, D.; Sels, B.; Song, J.; Chen, L.; Zhang, T.; Tang, P.; Morante, J. R.; Arbiol, J.; Fransaer, J., From rational design of a new bimetallic MOF family with tunable linkers to OER catalysts. *Journal of Materials Chemistry A* **2019**, *7* (4), 1616-1628.
8. Vijayakumar, E.; Ramakrishnan, S.; Sathiskumar, C.; Yoo, D. J.; Balamurugan, J.; Noh, H. S.; Kwon, D.; Kim, Y. H.; Lee, H., MOF-derived CoP-nitrogen-doped carbon@NiFeP nanoflakes as an efficient and durable electrocatalyst with multiple catalytically active sites for OER, HER, ORR and rechargeable zinc-air batteries. *Chemical Engineering Journal* **2022**, *428*.
9. Dou, S.; Li, X.; Tao, L.; Huo, J.; Wang, S., Cobalt nanoparticle-embedded carbon nanotube/porous carbon hybrid derived from MOF-encapsulated Co₃O₄ for oxygen electrocatalysis. *Chem Commun (Camb)* **2016**, *52* (62), 9727-30.
10. Pan, Y.; Wang, M.; Li, M.; Sun, G.; Chen, Y.; Liu, Y.; Zhu, W.; Wang, B., In-situ construction of N-doped carbon nanosnakes encapsulated FeCoSe nanoparticles as efficient bifunctional electrocatalyst for overall water splitting. *Journal of Energy Chemistry* **2021**.
11. Xiong, D.; Lu, C.; Chen, C.; Wang, J.; Kong, Y.; Liu, T.; Ying, S.; Yi, F.-Y., CoFeP nanocube-arrays based on Prussian blue analogues for accelerated oxygen evolution electrocatalysis. *Journal of Power Sources* **2022**, *520*.
12. Yuan, C. Z.; Sun, Z. T.; Jiang, Y. F.; Yang, Z. K.; Jiang, N.; Zhao, Z. W.; Qazi, U. Y.; Zhang, W. H.; Xu, A. W., One-Step In Situ Growth of Iron-Nickel Sulfide

Nanosheets on FeNi Alloy Foils: High-Performance and Self-Supported Electrodes for Water Oxidation. *Small* **2017**, *13* (18).

13. Hong, W.; Kitta, M.; Xu, Q., Bimetallic MOF-Derived FeCo-P/C Nanocomposites as Efficient Catalysts for Oxygen Evolution Reaction. *Small Methods* **2018**, *2* (12).

14. Bai, Y.; Zhang, L. C.; Li, Q.; Wu, Y.; Wang, Y.; Xu, M.; Bao, S. J., Self-Supported CdP2-CDs-CoP for High-Performance OER Catalysts. *ACS Sustainable Chemistry & Engineering* **2021**, *9* (3), 1297-1303.

15. Zha, M.; Pei, C.; Wang, Q.; Hu, G.; Feng, L., Electrochemical oxygen evolution reaction efficiently boosted by selective fluoridation of FeNi₃ alloy/oxide hybrid. *Journal of Energy Chemistry* **2020**, *47*, 166-171.

16. Liu, Z.; Yu, X.; Yu, H.; Xue, H.; Feng, L., Nanostructured FeNi₃ Incorporated with Carbon Doped with Multiple Nonmetal Elements for the Oxygen Evolution Reaction. *ChemSusChem* **2018**, *11* (16), 2703-2709.

17. Wang, Z.; Ang, J.; Zhang, B.; Zhang, Y.; Ma, X. Y. D.; Yan, T.; Liu, J.; Che, B.; Huang, Y.; Lu, X., FeCo/FeCoNi/N-doped carbon nanotubes grafted polyhedron-derived hybrid fibers as bifunctional oxygen electrocatalysts for durable rechargeable zinc-air battery. *Applied Catalysis B: Environmental* **2019**, *254*, 26-36.

18. Kai, C.; Seonghee, K.; Rajmohan, R.; Kandasamy, P.; Guan, Li.; Zhi, S.; Chan, J.; Jun, K.; Oi, L., Enhancing ORR/OER active sites through lattice distortion of Fe-enriched FeNi₃ intermetallic nanoparticles doped N-doped carbon for high-performance rechargeable Zn-air battery. *J. Colloid Interface Sci.* **2021**, *582*, 977-990.